Diffraction-like Synthetic Functions to Treat the Scattering from Large Polyhedral Metallic Objects

Massimiliano Casaletti [1], Stefano Maci [1], and Giuseppe Vecchi [2]
[1] Department of Information Engineering
University of Siena, Siena, Italy
casaletti@dii.unisi.it , macis@dii.unisi.it

[2] LACE Department of Electronics
Politecnico di Torino, Torino, Italy
giuseppe.vecchi@polito.it

***Abstract*—** This paper presents an innovative procedure that allow for the Method of Moments (MoM) analysis of electrically large objects composed of flat faces, i.e. open or closed polyhedrons with or without attached plates. The method is framed within the category of iteration-free, compressive basis function approaches. Two kinds of diffraction-like basis functions are introduced to achieve drastic memory requirement compression; relevant results compared with those obtained employing standard RWG basis functions are presented.

***Index Terms*—** Method of Moment (MoM), large structures, Synthetic Functions (SFX), scattering.

I. INTRODUCTION

The Integral Equation (IE) approach combined with the Method of the Moment (MoM) discretization scheme is widely used in the prediction of the electromagnetic scattering from a large complex objects. The conventional MoM formulations have well-known limits to the problem size, because they lead to large, dense and sometimes ill-conditioned matrices, with a consequent huge memory occupation and CPU time consumption. In order to overcome these problems, different schemes have been presented in literature. Among these schemes, we mention the Fast Multipole Method (FMM), the Adaptive Integral Method (AIM), and the multilevel matrix decomposition algorithm.

An alternative route is taken in a family of methods that employ an "iteration free" approach [1], where standard (e.g. RWG) basis functions are aggregated into larger functions. This notably includes the Synthetic Function expansion (SFX) [2] and the Characteristic Basis Function (CBF) [3] methods. These aggregate basis functions are defined from the solution of smaller-size numerically-tractable problems, excited by appropriate sources, and then used in the MoM solution of the large problem. This allows one to incorporate the intermediate and macro-scale features of the structure, while maintaining a reduced number of unknowns. Thousand of wavelength structures can be treated with memory and CPU cost provided by a standard personal computer. Within this scheme, we proposed here a method to treat large portions of PEC planar objects containing edges; special cases include geometries with large polyhedral sub-surfaces, as frequently encountered in ships and especially in satellites. We will show that this appears a quite useful addition to the general framework of the iteration free methods.

The core of the proposed method is centered around the construction of the basis functions that describe the edge diffraction effects. As usual in compressive methods, the large-support basis functions derive from the (exact or approximate) solution of the EM problem on portions of the overall structure, for a set of suitable excitations. A key issue investigated here is the excitation mechanism employed to generate these basis functions. Two different approaches are investigated, and the relevant results critically compared: 1) spherical wave generated diffraction basis functions where the generating dipoles are located slightly displaced from the edge; 2)

grazing plane-wave generated BF with different propagation directions.

The paper is structured as follows: in Section II, the iteration free synthetic function method is summarized to frame the present approach; the particular case of flat metallic portions and of the object within the Physical Optics interpretation is discussed. In Section III, the appropriate definitions of the two types of generating sources for defining the basis functions is presented. Section IV shows the procedure to select and construct the synthetic basis functions on the basis of the singular value decomposition, and the subsequent followed Section V illustrate the MoM spectral domain solution, with focus on the calculation of the impedance matrix entries. Numerical results are presented in Section VI.

II. THE SFX METHOD

In the following, we will start from the baseline SFX method. The first step is a geometrical domain-decomposition, that breaks down the conductor surface into portions, that we called surface blocks (s-blocks) S_i, whose collection reconstruct the entire surface S on which EFIE is applied. Each s-block is bounded by a boundary line ∂S_i. On each s-block S_i, one generates basis functions with support on the entire s-block, that are subsequently used as synthetic basis functions (SBF) for the analysis of the entire structure. Since the number of SBF functions is significantly smaller than those used in a conventional description [4], the overall number of unknowns is drastically reduced with a consequent gain in terms of memory and solution time. These basis functions defined over the entire domain S_i are called "Synthetic Functions" (SF), they are generated from the numerical solution of the electromagnetic problem for the block in isolation, under excitation by suitably defined "generating" sources. The synthetic functions are obtained from a linear combination of the responses to all sources via a procedure based on the Singular-Value Decomposition (SVD). Because of the strong reduction of the global number of unknowns, one can store the MoM matrix and afford a direct solution. In this sense, the method can be viewed as an "iteration-free" alternative to so-called fast methods (like the Fast Multiple Method) that are based on iterative solvers for the MoM linear system, and on special techniques to avoid the storage of the full MoM matrix. The method is kernel-free, and can be implemented on top of existing MoM codes.

A. Flat Perfectly Conducting Portions of Complex Objects

Let us assume as an s-block a flat perfectly conducting portion of surface. If the geometrical decomposition conforms to the mesh of the entire structure the boundary line ∂S may result in zigzag lines to conform to the mesh edges (see surface S_i in Fig. 1). The way to treat interaction among blocks with non-straight contour ∂S mesh is described in [4] and will not be repeated here. For the sake of simplicity, we will assume here that the boundary line ∂S is composed by straight segments (see surface S_i in Fig. 1); this is not a restriction, except on the meshing algorithm (the meshing should follow the block subdivision and not vice-versa). As described for the general scheme [4], the s-block (flat polygonal face) is isolated from the rest of the structure by a (virtual) closed surface S^{eq} (bounding box), via the Equivalence Theorem. On this separation surface one then allows an equivalent current distribution that accounts for the external world. This equivalent current distribution may be defined by using several kinds of wave objects, like plane waves [3], point sources [4], or complex point sources. The SFX formulation *does not* use the coefficient of these wave objects as unknowns of the problem. Rather it use these sources as *generating sources* for the basis functions to be defined on for the s-block, called Synthetic Functions (SF). The set of EM responses to the generating sources constitutes the starting point for the generation of the SF set, in which a SVD is employed to orthogonalize and discriminate among the totality of the responses that might have scarce linear independence.

As mentioned before the choice of the generating sources is largely arbitrary [4], and different sets of (synthetic) basis functions arise from different choices of generating sources. The efficiency of each scheme, i.e. the number of necessary SF to represent the solution to the complete problem is actually associated to the ability of the generating sources to produce responses that well reconstruct the solution space,

the latter being defined as the (sub) space spanned by all the possible solutions for the entire problem localized to the considered s-block.

B. Physical Optics SF

When addressing the internal part of the equivalence problem for the s-block, the (arbitrary) medium that can fill the external part is chosen in order to simplify as much as possible the Green's function of the internal region. The conventional choice is to fill the external region by a free-space medium. In this case, the SF basis functions f_n are derived by a MoM solution of a problem of the dimension of the surface block in isolation. Taking advantage from the fact that our s-block is a flat surface, the region external to S^{eq} is filled with the infinite continuation of the flat portion, to recover an infinite flat plate (see Fig. 1). This allows the construction of the SF f_i in exact closed form for each generating source, simply applying the image principle. The responses so obtained will be called "PO functions" in the following. Because of the simplicity of dealing with analytical expressions of PO functions, in the following we will use the PO functions as starting point for the generation of SF on flat polygonal plates. The usual SVD process [4] will be used on them to generate the actual SF.

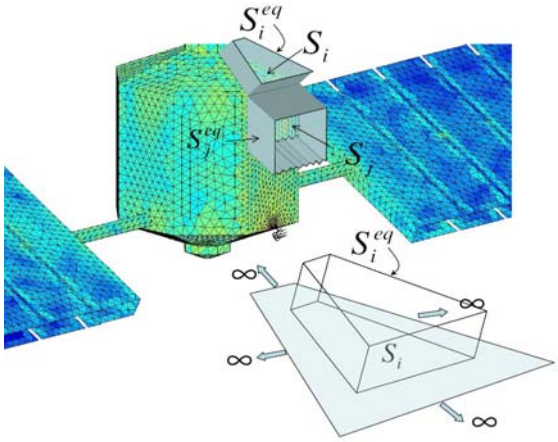

Fig. 1. Flat surface blocks on complex object. The surface block S_i is bounded by true edges; part of the contour of the surface block S_j matches the mesh edges. The surface blocks are isolated by equivalent surface S_i^{eq}; the exterior of this surface is filled by the infinite continuation of the flat surface to simplify the internal region.

As generating sources we will use and compare both grazing plane waves and point sources (dipoles); this is addressed in the next sections.

In order to avoid confusion, in the following we will always deal with a block subdivision in which the edges of the s-block correspond to actual edges in the overall structure. This is the sensible choice for this approach, but it is obviously different from the setting in [4], where large plates could be "torn" into smaller pieces to reduce the associated computational effort. The singular behavior of the field at these edges is therefore not an artifact of the procedure in this case.

III. GENERATING SOURCES AND THEIR SPACE AND SPECTRAL RESPONSES

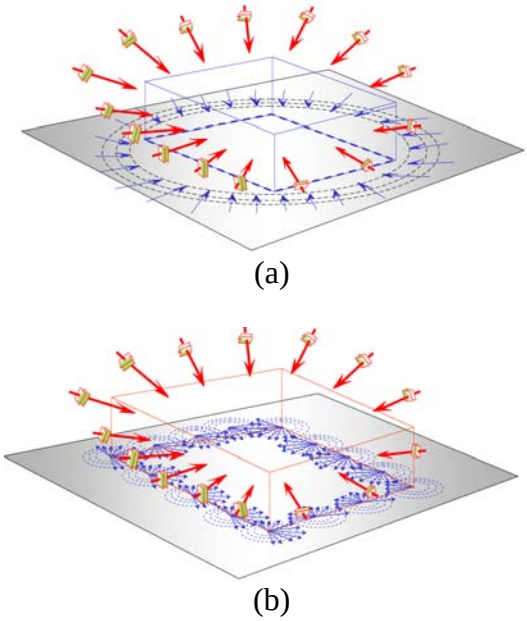

Fig. 2. Different schemes for generating PO synthetic basis functions. (a) Homogeneous plane waves plus nearly evanescent plane waves, (b) homogeneous plane waves plus spherical wave sources.

The choice of the generating sources is a key point for the correct reconstruction of the solution space. Let us subdivide conceptually the current solution J on the s-block in the sum of two contributions $J_0 + J_f$, where J_f are the "fringe" currents associated to the diffraction process at the true edge of the S-block, and J_0 is the remainder. Two schemes will be investigated here.

In a first scheme the solution space associated to the fringe currents J_f will be spanned by synthetic functions generated by *elementary dipoles* distributed close to the edges of the S-block. The synthetic functions to describe the remainder contribution J_0 are instead generated by *homogeneous plane waves* . In a second scheme, the contribution J_0 is still represented by SFs generated by homogeneous plane waves, while the fringe contributions are generated by *nearly-evanescent (near grazing) plane waves*. The two schemes differ in the way to describe the fringe contributions. We have set our focus on the diffraction effects, and therefore we limit our investigation here on the contribution J_f described by the two mentioned alternatives.

A. Spherical Wave Generation of Po Basis Functions

As prescribed in the framework of high frequency diffraction theory, the diffraction process may be described by equivalent spherical wave incremental contributions arising from the edge [5, 6]. Following this guideline, it seems adequate the use of (elementary) dipoles distributed close to the edge as generating sources of fringe currents. To this end, let us introduce a local reference system with the τ-axis along the considered edge of the surface, the η-axis orthogonal to the edge oriented toward the surface and z-axis normal to the surface, that lies at $z=0$ (see Fig. 3).

The generating electric dipoles are centered at a generic position τ' and displaced of $\lambda/10$ from the edge along both τ and η in order to avoid inappropriate singularities at the edge. To cover the two polarizations, pairs of dipoles parallel and orthogonal to the edge are used. The PO induced currents normalized with respect to the maximum values can be well approximated by the following expressions:

$$\begin{Bmatrix}\mathbf{f}_\tau(x',x,y)\\ \mathbf{f}_\eta(x',x,y)\end{Bmatrix}=\sum_m \frac{\alpha}{\pi\lambda}\frac{e^{-jkr_m}}{r_m}\left(1-\tfrac{1}{kr_m}\right)\chi(x,y)\cdot\begin{Bmatrix}\hat{\boldsymbol{\tau}}_m\\ \hat{\boldsymbol{\eta}}_m\end{Bmatrix}, \quad (1)$$

where: $\hat{\boldsymbol{\tau}}_m=\hat{\mathbf{s}}_m^-=\dfrac{(\mathbf{v}_{m+1}-\mathbf{v}_m)}{|\mathbf{v}_{m+1}-\mathbf{v}_m|}$, $\hat{\boldsymbol{\eta}}_m=\hat{\mathbf{z}}\times\hat{\mathbf{s}}_m^-$,

$r_m=\sqrt{(\tau-\tau')^2+(\eta-\lambda/10)^2+(\lambda/10)^2}$,

$\hat{\mathbf{s}}_m^-=\dfrac{(\mathbf{v}_{m+1}-\mathbf{v}_m)}{|\mathbf{v}_{m+1}-\mathbf{v}_m|}$, $\mathbf{v}_m$ (m=1,.. N) are the position vectors of the s-block surface vertexes, α is the normalization constant that is taken to have maximum amplitude equal to unity, and $\chi(x,y)$ is the characteristic function of the s-block, that is unity inside the s-block and zero elsewhere. The basis functions are normalized in such a way that the maximum value of the amplitude (obtained for $\eta=0$, and $\tau=\tau'$) is equal to unity. The generating sources are placed along the polygonal contour of the surface with uniform steps, thus constructing a sequence of type:

$$\mathbf{f}_{n,\xi}(x,y)=\mathbf{f}_\xi(n\delta,x,y)=$$
$$=\frac{25}{\pi\lambda}\sum_m\frac{e^{-jkr_n}}{r_n}\left(1-\tfrac{1}{kr_n}\right)\chi(x,y)\hat{\boldsymbol{\xi}}_m, \quad (2)$$

where: $\hat{\boldsymbol{\xi}}_m=\hat{\boldsymbol{\tau}}_m,\hat{\boldsymbol{\eta}}_m$

$r_n=\sqrt{(\tau-n\delta)^2+(\eta-\lambda/10)^2+(\lambda/10)^2}$.

Since the currents are devoted to reconstruct diffraction effects, these functions are herein after denoted as *Spherical wave generated-PO functions (SWG-POF)* . The step δ between contiguous generating sources will be chosen according to the SVD scheme presented in the subsequent section.

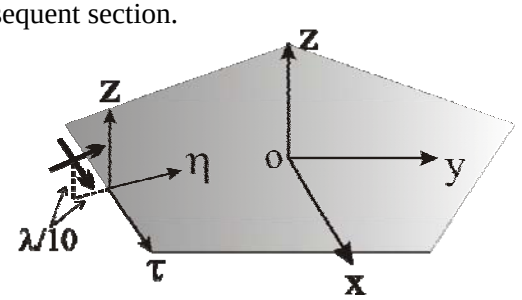

Fig. 3. Geometry for defining SWG-POF.

It is interesting to look at the Fourier transform

$$\tilde{\mathbf{F}}_{n,\xi}(k_x,k_y)=FT[\mathbf{f}_{n,\xi}(x,y)] \quad (3)$$

of the two types of PO-functions. Note that the spectrum is not available in closed form due to the presence of the truncation function $\chi(x,y)$; therefore an FFT has been used to calculate it. The typical spectral domain behavior of $\left|\tilde{\mathbf{F}}_{n,\xi}(k_x,k_y)\right|$

for the case of a flat metallic square s-block is shown in Fig. 4, while the space domain response is strongly concentrated in the area close to the generating dipole, the spectral amplitude is concentrated close in an angular spectral sector around the circular periphery of the visible region (Fig. 4). Note that the extension of the significant spectral region is different when the source is near a corner and when it is near a fault edge. These spectra can be simply explained (at least inside the visible region) by invoking the direct relationship between the far field radiated by each basis function and the spectrum of the same basis function. It is indeed evident that the PO field scattered by a metallic plate illuminated by a coplanar dipole is concentrated in the paraxial region, with an angular spread which is dictated by the metallic sector seen by the generating source in its actual position; it is also useful to recall that the boundary of the visible region in (k_x, k_y) corresponds to grazing directions. For instance, if the dipole is placed on a corner of the first quadrant of a square plate, the far field radiation density (spectrum amplitude) is concentrated in the opposite direction (third quadrant of the spectral plane) close to grazing aspect (boundary of the visible region) and along an angular range of 90°. If the source is placed at the center of the edge, the radiation is concentrated along an angular range of 180° in the opposite directions. The spectral density concentration will be used to derive a criterion to select the right number of generating sources to be placed around the s-block periphery (see Section IV).

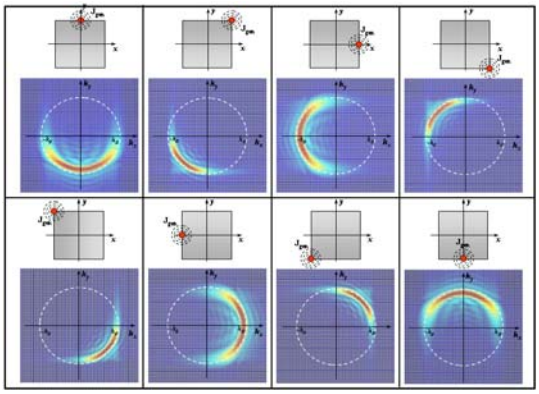

Fig. 4. Spectrum amplitude of the diffraction basis functions for a given position of the spherical wave generating sources.

B. Nearly Grazing Plane Wave Generation of PO Basis Functions

An alternative description of the diffraction contribution can be given in terms of basis functions generated by propagating nearly grazing plane waves. As a generating source we take TE or TM polarized plane waves characterized by the wave-vector $\mathbf{k}' = \mathbf{k}_t' + \mathbf{z}\sqrt{k - \left(k_x'\right)^2 - \left(k_y'\right)^2}$, where $\mathbf{k}_t' = k_x'\hat{\mathbf{x}} + k_y'\hat{\mathbf{y}}$ is the transverse to z part of $\mathbf{k}'$, and k is the free-space wave-number. The transverse wave-vectors $\mathbf{k}_t'$ associated to the generating plane waves are chosen so that $k^2 \tilde{<} \left(k_x'\right)^2 + \left(k_y'\right)^2$ (near grazing incidence) with a constant angular step; namely

$$\mathbf{k}_{tn}' = k\left(\sin\left(n\Delta\phi\right)\hat{\mathbf{x}} + \cos\left(n\Delta\phi\right)\hat{\mathbf{y}}\right), \qquad (4)$$

where the step $\Delta\phi$ between contiguous wave-numbers will be chosen according to the SVD scheme presented in the next section and in a similar way as done for the selection of the spherical wave basis functions. The normalized PO currents associated to the above plane waves are given by

$$\begin{aligned} \mathbf{f}_{n,TM}(\mathbf{k}', x, y) &= \mathbf{k}_{tn}' e^{-j(k_x' x + k_x' y)} \chi(x, y), \\ \mathbf{f}_{n,TE}(\mathbf{k}', x, y) &= \mathbf{k}_{tn}' \times \hat{\mathbf{z}} e^{-j(k_x' x + k_x' y)} \chi(x, y), \end{aligned} \qquad (5)$$

where χ is the above-defined characteristic function of the polygonal surface. We note that in order to interpret the TE component in (5) as a normalized grazing wave PO current for TE polarization, we should apply a process to the limit for near grazing of the normalized currents. We note indeed that the non-normalized TE PO currents are zero for exact grazing incidence, but the TE component are essential to the completeness of the description. The spectrum of the above functions can be evaluated in a closed form for arbitrary polygonal flat surface with vertexes located at the position vectors $\mathbf{v}_m$ (m=1,.. N), as

$$\begin{aligned} \tilde{\mathbf{F}}_{n,TM}\left(k_x, k_y\right) &= -j \frac{\mathbf{k}_{tn}'}{k\left|\mathbf{w}_n\right|^2} \sum_{m=1}^{N} T_{n,m}(k_x, k_y), \\ \tilde{\mathbf{F}}_{n,TE}\left(k_x, k_y\right) &= -j \frac{\mathbf{k}_{tn}' \times \hat{\mathbf{z}}}{k\left|\mathbf{w}_n\right|^2} \sum_{m=1}^{N} T_{n,m}(k_x, k_y), \end{aligned} \qquad (6)$$

where

$$T_{n,m}(k_x,k_y)=\left(\mathbf{w}_n^{\ *}\cdot\mathbf{s}_m^{-}\right)e^{j\frac{k}{2}\mathbf{w}_n\cdot\mathbf{s}_m^{+}}\frac{\sin\left(\frac{k}{2}\mathbf{w}_n\cdot\mathbf{s}_m^{-}\right)}{\frac{k}{2}\mathbf{w}_n\cdot\mathbf{s}_m^{-}}, \quad (7)$$

in which

$$\mathbf{w}_n=(\mathbf{k}_{tn}^{'}-\mathbf{k}_t)/k,$$
$$\mathbf{s}_m^{\pm}=\left(\mathbf{v}_{m+1}\pm\mathbf{v}_m\right). \quad (8)$$

The spectrum of each *plane wave generated PO functions* (PWG-POF) is concentrated along the boundary of the visible region and rotates at each angular increment $\Delta\phi$ in the direction of incidence of an equal spectral azimuthally step. Figure 5 illustrates the same case of a square plate used in for the spherical wave generation (Fig. 4). At difference with SWG-POF, here the spectral spot is azimuthally narrow, being the spectral density in both directions inversely proportional to the size of the domain in the corresponding spatial direction. This is well evident in case of a rectangular plate, because of the associated separable *sinc* spectral functions, and it holds in general.

Compared to the spherical wave functions, the present basis functions appear to be spectrally localized, while the previous functions were spatially localized; they are therefore complementary.

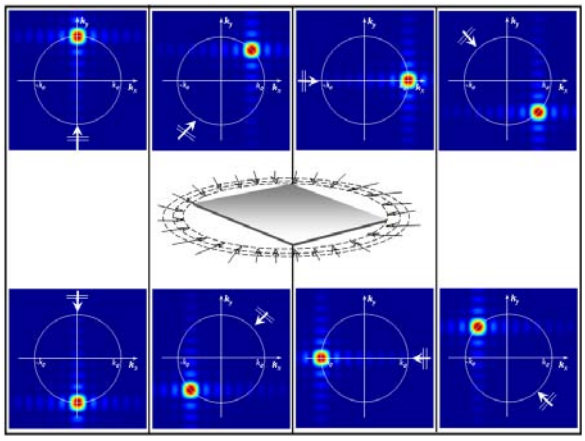

Fig. 5. Amplitude of the spectrum of the PO basis functions for a given direction of incidence of the plane wave generating sources for a four wavelength square plate. The associated plane wave direction is symbolically depicted in each same diagram.

IV. SINGULAR VALUE DECOMPOSITION (SVD) PROCESS

A. Selection of the Number of Generating Functions through SVD

The optimal number of basis functions is determined by evaluating the degree of independence of the entire domain functions both generated by near-edge dipoles and by near-grazing plane-waves via an iterated SVD-based procedure analogous to the one described in [4].

In the proposed procedure, we start with a given discretization in both schemes, i.e. with a given spatial (δ) or spectral ($\Delta\phi$) source density; the responses to the source sets are computed as indicated above, and processed by SVD as described in [4]. The number of the generating sources is incremented by reducing increasingly the parameter δ or $\Delta\phi$ with a linear law, and the SVD repeated. The process is stopped when the N most relevant SV do not change beyond a fixed ratio between the minimum and the maximum singular value, the latter can't be too small to avoid ill-conditioning.

At a difference with the procedure in [4], we adopt here a specialized implementation of the SVD generation process, that is very convenient for the present case. The procedure in [4] operates on the coefficients of the solution represented in terms of elemental, spatially localized functions (e.g. RWG), i.e. with spatial samples of the responses to the set of defining sources; in that case, the number of spatial samples is simply dictated by the mesh initially chosen to discretize the problem. In the present case, the (PO) responses are not subjected to an inherent spatial discretization, which is however a necessity when dealing with numerical operations. In the first place, then, we will choose a discretization for the PO responses to dipoles and plane waves; we will use $2N_s$ samples, being only constrained to be able to correctly represent the functions. In addition, we observe that in the present case it is meaningful and feasible to employ *spectral* samples instead of spatial samples of the responses. Indeed, the natural space sampling of the PO responses is not suitable since the s-block surface may extend over several wavelengths, thus leading to very large matrices. Furthermore, it has been shown in section III that both the spherical-

and the plane-wave generation processes produce responses with spectral concentration around the boundary of the visible region. This suggest a spectral sampling of the PO response spectra in N_s equal-spaced points on the spectral circumference of radius k (Fig.6).

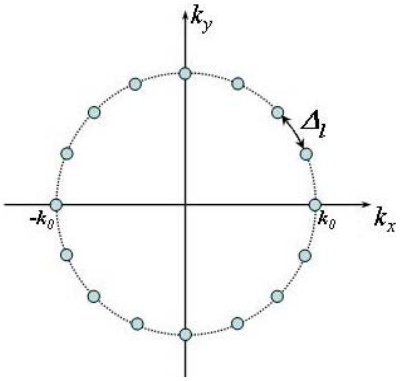

Fig. 6. Example of spectral samples for SVD computation.

We call N the number of employed sources, and we assemble the $2N_s$ samples (N_s samples for each polarization) of the ensuing N PO functions into the columns of the $2N_s \times N$ response matrix $\mathbf{R}$. This matrix represents the operator that maps the (N-dimensional) source spanned by linear combinations of the generating sources into the corresponding PO currents.

For spherical wave generating functions (dipole sources) the entries of the response matrix $\mathbf{R} = \left\{ r_{pq} \right\}_{\substack{p=1,2N_s \\ q=1,N}}$ are given by:

$$\begin{aligned} r_{2p'-1,2q'-1} &= \tilde{\mathbf{F}}_{q',\tau}(k_{sx},k_{sy}) \cdot \hat{\mathbf{x}} \\ r_{2p',2q'-1} &= \tilde{\mathbf{F}}_{q',\tau}(k_{sx},k_{sy}) \cdot \hat{\mathbf{y}} \\ r_{2p'-1,2q'} &= \tilde{\mathbf{F}}_{q',\eta}\left(k_{sx},k_{sy}\right) \cdot \hat{\mathbf{x}} \\ r_{2p',2q'} &= \tilde{\mathbf{F}}_{q',\eta}\left(k_{sx},k_{sy}\right) \cdot \hat{\mathbf{y}} \\ p' &= 1,\ldots,N_s, q' = 1,\ldots,\frac{N}{2}, \end{aligned} \tag{9}$$

where: $\tilde{\mathbf{F}}_{n,\xi}(k_x,k_y)$ is defined in (3), $k_{sx} = k_0 \cos\left(s\Delta\eta\right)$, $k_{sy} = k_0 \sin\left(s\Delta\eta\right)$, $\Delta\eta = 2\pi / N_s$ and $s = 1,\ldots,N_s$.

For near-grazing plane-wave sources they are given by:

$$\begin{aligned} r_{2p'-1,2q'-1} &= \tilde{\mathbf{F}}_{q',TE}\left(k_{px},k_{py}\right) \cdot \hat{\mathbf{x}} \\ r_{2p',2q'-1} &= \tilde{\mathbf{F}}_{q',TE}\left(k_{px},k_{py}\right) \cdot \hat{\mathbf{y}} \\ r_{2p'-1,2q'} &= \tilde{\mathbf{F}}_{q',TM}\left(k_{px},k_{py}\right) \cdot \hat{\mathbf{x}} \\ r_{2p',2q'} &= \tilde{\mathbf{F}}_{q',TM}\left(k_{px},k_{py}\right) \cdot \hat{\mathbf{y}} \\ p' &= 1,\ldots,N_s, q' = 1,\ldots,\frac{N}{2}, \end{aligned} \tag{10}$$

where $\tilde{\mathbf{F}}_{n,TE}$ and $\tilde{\mathbf{F}}_{n,TM}$ are defined in (6). Note that this scheme strongly reduces number of samples with respect to those needed in a space domain sampling. The number of samples N_s has to be greater than N and sufficiently large to respect the Shannon sampling condition (correct representation of the spectral current functions); namely $N_s \geq \lfloor 2\pi k_0 / 2B \rfloor$, where B is the larger extension of the total surface.

Applying to the matrix $\mathbf{R}$ the SVD process yields the decomposition

$$\mathbf{R} = \mathbf{U}\Sigma\mathbf{V}^H, \tag{11}$$

where $\mathbf{U}$ and $\mathbf{V}$ are unitary matrix and Σ is the diagonal matrix containing the singular values $\sigma_1 \geq \sigma_2 \geq \cdots \geq \sigma_N$. The shape of this decomposition is visualized below for convenience of the reader

$$\mathbf{R} = \mathbf{U} \begin{bmatrix} \sigma_1 & 0 & 0 & 0 \\ 0 & \sigma_1 & 0 & 0 \\ 0 & 0 & \ldots & \\ 0 & 0 & 0 & \sigma_N \end{bmatrix} \mathbf{V}^H$$

The square matrices $\mathbf{U} = \left\{ u_{ij} \right\}_{\substack{i=1,2N_s \\ j=1,2N_s}}$ and $\mathbf{V} = \left\{ v_{nm} \right\}_{\substack{n=1,N \\ m=1,N}}$ have dimensions $2N_s$ and N, respectively, and the matrix Σ has and the same dimensions $2N_s \times N$ as $\mathbf{R}$. The matrix $\mathbf{V}^H = \left\{ v^*_{mn} \right\}_{\substack{n=1,N \\ m=1,N}}$ is the transpose conjugate of $\mathbf{V}$.

The singular value sequence $\left\{ \sigma_i \right\}$ typically presents a decay beyond a certain value [7].

As indicated in [4], the normalized SV sequence σ_r / σ_1 indicates the relative independence of the r^{th} singular vector respect to the preceding subset, is a good indicator to select the necessary number of synthetic functions, upon the establishment of a threshold. For a given N, we increase iteratively the number of the

generating sources, recomputing the SVD and stopping the process when the SV within the thresholding set of $\sigma_{\min}/\sigma_{\max}$ do not change anymore appreciably. A systematic implementation is based on the following iterative steps. One first fix an a priori value of $\sigma_{\min}/\sigma_{\max}$ on the basis of the conditioning number one can accept (let us say 10^{-4}). Next, one fix an initial number of generating sources $N = N_0$ on the basis of an initial guess for δ_0 (for SWG-BF) or $\Delta\phi_0$ (for PWG-POF). (for SWG-POF, $N_0 = P/\delta_0$ where P is the surface perimeter, for PWG-POF $N_0 = 360°/\Delta\phi_0$). As initial guess of the process we suggest $\delta_0 = \lambda/2$ and $\Delta\phi_0 = 30°$. Successively, the corresponding SV are determined trough (11). At the i^{th} iterative step the number of sources is increased to $N_i = 2N_{i-1}$ ($\delta_i = \delta_{i-1}/2$ or $\Delta\phi_i = \Delta\phi_{i-1}/2$) and the process is restarted obtaining a new SV sequence that is in general slightly different from that obtained at the previous step. The procedure is stopped when the SV sequence inside the fixed threshold $\sigma_{\min}/\sigma_{\max}$ does not change appreciably anymore. We note that to stabilize the process we need a number of generating sources N_I (with I number of iterations) which is higher than the number $\overline{N}$ to which the sequence meets the threshold. Examples of stabilized SV sequences for PWG and SWG basis functions are shown in Fig. 7 and Fig. 8, respectively. The sequences are relevant to the problem of a square flat metallic plate of side 0.9λ. The horizontal axis presents the index number of singular values and the vertical axis the relevant normalized SV's. Fig. 7(a) are obtained sampling both TE- and TM-polarized waves at the same spectral locations. In Fig.7(b) only TE waves have been considered, with the evident outcome to reduce by a factor 2 the number of independent functions. Analogously, Fig. 8 are relevant to spherical generating dipoles both orthogonal and tangent to the edge (a) and only tangent to the edge (b). Again, the number of independent functions is reduced of a factor two in the second case. The final outcome of this analysis is that 60 PWG-POF are required to stabilized a sequence of 26 SV's in the range $\sigma_{\min}/\sigma_{\max} = 10^{-4}$, while in the same range, the required SWG-POF are 40 to stabilize a sequence of 34 SV's.

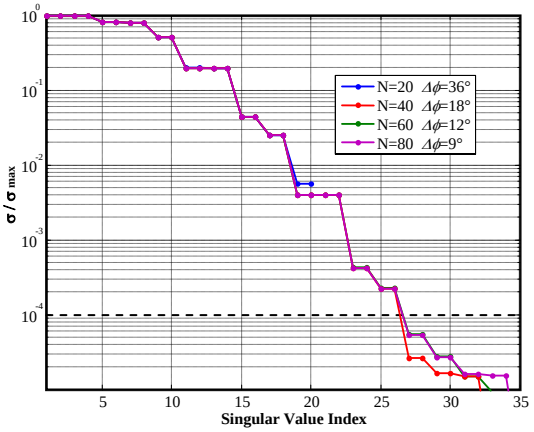

(a)

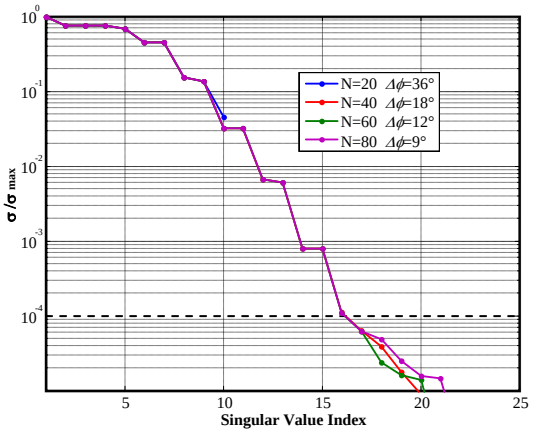

(b)

Fig. 7. Singular value sequences for PWG-POF defined over a square metallic plate of side length 0.9λ. The results are obtained using both polarization TE and TM (a) or using just the TE polarization (b). The spectral step $\Delta\phi$ is decreased till when each sequence is stabilized in the range $\sigma/\sigma_{\max} = 10^{-4}$. The final step $\Delta\phi$ obtained is $\Delta\phi = 12°$.

B. Generation of the Synthetic Functions

The final SVD obtained at the end of the iterative process contains information of an "orthogonal" set of synthetic functions in spectral (in the $\mathbf{U} = \{u_{ij}\}_{\substack{i=1,2N_s \\ j=1,2N_s}}$) and spatial (in the matrix $\mathbf{V} = \{v_{nm}\}_{\substack{n=1,N \\ m=1,N}}$) domain, where N is the number of generating sources used to stabilized the sequence.

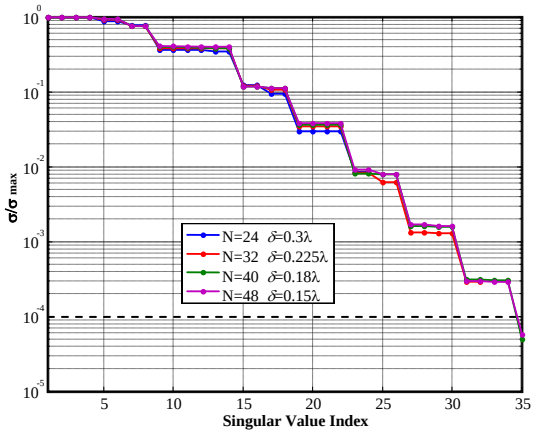

(a)

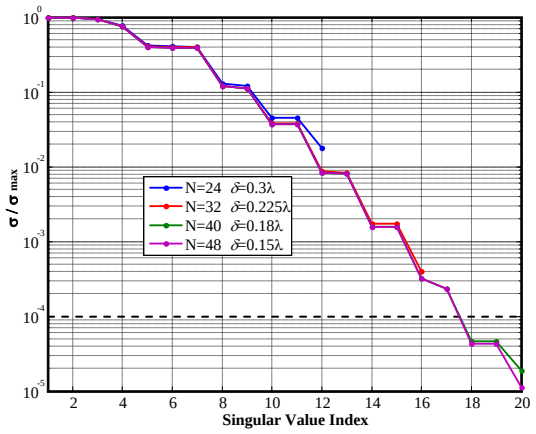

(b)

Fig. 8. Singular value sequences for SWG-POF defined over a squared metallic plate of side length 0.9λ obtained using both polarized dipoles as generating sources (a) or using only dipoles alignment to the edge (b). The space step δ is decreased till when each sequence is stabilized in the range $\sigma/\sigma_{\max}=10^{-4}$. The finale δ-step obtained is 0.18λ.

In particular, the coefficients of the n^{th} column of $\mathbf{V}$ constitutes the coefficients of the PO-type functions that synthesize orthonormal *plane-wave generated synthetic basis functions* (PWG-SFX) or *spherical-wave generated synthetic basis functions* (SWG-SFX) in spatial domain:

$$\mathbf{d}_m(x,y)=\frac{1}{\sigma_m}\sum_{n'=1}^{N/2} v_{(2n'-1),m}\mathbf{f}_{n',\zeta_1}(x,y) + v_{2n',m}\mathbf{f}_{n',\zeta_2}(x,y) \quad (12)$$

$$m=1,\ldots,\bar{N},$$

$$\zeta_1=\begin{cases} TE & \text{for PWG-SFX} \\ \tau & \text{for SWG-SFX} \end{cases},$$

$$\zeta_2=\begin{cases} TM & \text{for PWG-SFX} \\ \eta & \text{for SWG-SFX} \end{cases}.$$

The number of synthetic functions $\bar{N}$ corresponds to the number of singular value inside the dynamic range (e.g. $\bar{N}=26$ for PWG-SBF, and $\bar{N}=35$ for SWG-SBF in case of Figs. 7 and 8). The spectrum of the selected synthetic functions can be easily obtained by linearity from the spectrum of the generating sources:

$$\tilde{\mathbf{D}}_{m,\zeta}(k_x,k_y)=\frac{1}{\sigma_m}\sum_{n'=1}^{N/2} v_{(2n'-1),m}\tilde{\mathbf{F}}_{n',\zeta_1}(k_x,k_y) + v_{2n',m}\tilde{\mathbf{F}}_{n',\zeta_2}(k_x,k_y) \quad (13)$$

$m=1,\ldots,\bar{N}.$

We note that sampling the above equality on the boundary of the visible spectral region in the same N_s spectral points used for the SVD in (11) reconstructs the relation $\mathbf{RV}=\mathbf{U}\Sigma$ obtained by multiplying both sides of (11) by $\mathbf{V}$ (note that $\mathbf{V}^{-1}=\mathbf{V}^H$). We note that the spherical wave generation approach requires in general less number of sources to reach a stable value of the SV sequence wrt the plane wave generation , the latter really finally gives a lower number of SV's within the same threshold, after stabilization of the sequence.

V. MOM SOLUTION

The basis function selected by the SVD process are now used in a MoM-Galerkin solution scheme. Since the synthetic functions are extended over domains that could be electrically large, it is convenient the use of the inverse spectral-domain transform of the MoM matrix entries. Our investigation is limited here to coplanar basis functions, but the process should be easily extended to non coplanar surfaces [8, 9]. For a pair of two spectral synthetic functions $\tilde{\mathbf{D}}_{p,\zeta}$ and $\tilde{\mathbf{D}}_{q,\eta}$ the Galerkin MoM matrix entry is obtained as

$$Z_{pq}^{\zeta\sigma}=-\frac{\varsigma\kappa}{8\pi^2}\int_{-\infty}^{+\infty}\int_{-\infty}^{+\infty}\tilde{\mathbf{D}}_{p,\zeta}(k_x,k_y)\cdot\frac{1}{k_z}\left[\underline{\underline{I}}-\frac{\mathbf{kk}}{{\kappa_0}^2}\right]\cdot\tilde{\mathbf{D}}_{q,\sigma}(-k_x,-k_y)\,dk_x dk_y \quad (14)$$

$p,q=1,\ldots,\bar{N},$

where $\mathbf{k} = k_x\hat{x} + k_y\hat{y} + k_z\hat{z}$ in which $k_z = \sqrt{k^2 - k_x^2 - k_y^2}$ is the wave-vector and ς is the characteristic impedance of the medium. Using (13), (14) can be expressed as a function of the mutual impedances $Z_{pq}^{\zeta\eta,PO}$ of the PO-type basis functions via

$$Z_{pq}^{\zeta\sigma} = \frac{1}{\sigma_p}\frac{1}{\sigma_q}\sum_{n=1}^{N}\sum_{n'=1}^{N} v_{n'q} v_{np} Z_{pq}^{\zeta\sigma,PO}, \tag{15}$$

$$Z_{pq}^{\zeta\sigma,PO} = -\frac{\varsigma\kappa}{8\pi^2}\int_{-\infty}^{+\infty}\int_{-\infty}^{+\infty} \tilde{\mathbf{F}}_{p,\zeta}\left(k_x, k_y\right) \cdot \frac{1}{k_z}\left[\underline{\underline{I}} - \frac{\mathbf{kk}}{\kappa_0^{\,2}}\right]\cdot \tilde{\mathbf{F}}_{q,\eta}\left(-k_x, -k_y\right) dk_x dk_y. \tag{16}$$

We stress that the integrand in (16) is calculated in a closed form for the plane wave generation approach and by FFT for the spherical wave generation approach.

VI. NUMERICAL RESULTS

As an example of application we consider a square flat plate of dimension $L = 0.9\lambda$ illuminated by an electric dipole at a distance of a wavelength as shown in Fig. 9. The plate will be considered as a unique block in the iteration-free procedure. The SVD sequences associated to this block for both type of basis function introduced in this paper are those shown in Figs. 7 and 8.

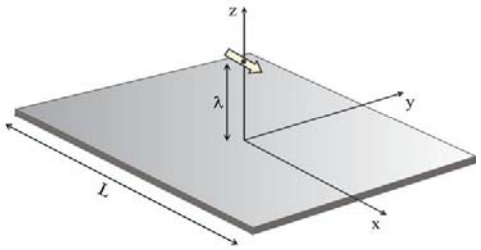

Fig. 9. Electric dipole radiating over a squared flat metallic plate.

The simulations have been carried out by using alternatively 26 PWG synthetic functions and 35 SWG synthetic basis functions, according to the sequence in Figs. 7a and 8a, respectively, and adding as a basis function a part the PO currents. The results compared with those provided by a commercial standard MoM (FEKO™) using 648 RWG basis functions. Figure 10 shows the amplitude of the induced currents on the plate in the E and H cut-planes. A reasonable good agreement has been seen except very close to the edge, where the SWG-SFX looks like more appropriate than PWG-SFX to represent the edge effect for the intrinsic space high resolution capability of the SWG-POF space functions.

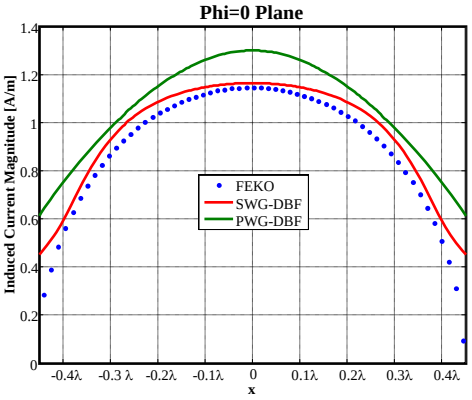

(a)

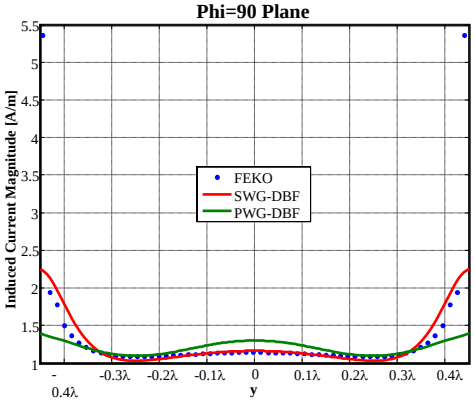

(b)

Fig. 10. Square plate, $L = 0.9\lambda$; comparison of the induced currents on (a) E-plane and (b)H-plane cuts.

Figure 11 shows the comparison between the far field in E-plane (Fig. 11a) and H-plane (Fig. 11b); the agreement is satisfactory for both SWG-DBF and PWG-DBF.

We observe that the present procedure increases accuracy for increasing the plate dimensions. Let us consider the same scattering problem as shown in Fig. 9 for a plate side $L = 4\lambda$. The simulations have been done by using 98 SWG-SFX and 80 PWG-SFX stabilized by using 120 SWG-POF and 100 PWG-POF, respectively; the relative SV sequences are shown in Fig. 12.

Figeurs13 and 14 shows the comparison of the far field and the induced current with a standard MoM (FEKO™) using 12800 RWG basis functions, as we can see using just respectively 98 SWG-SFX and 80 PWG-SFX it is possible to obtain a very good agreement between the results.

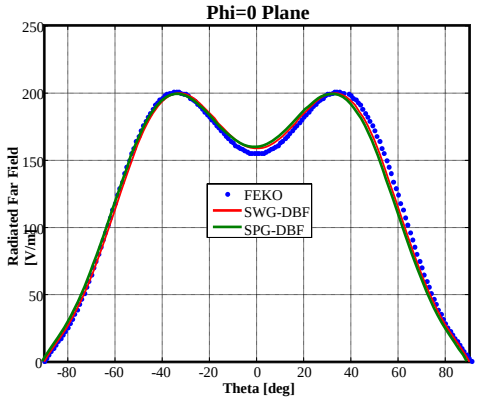

(a)

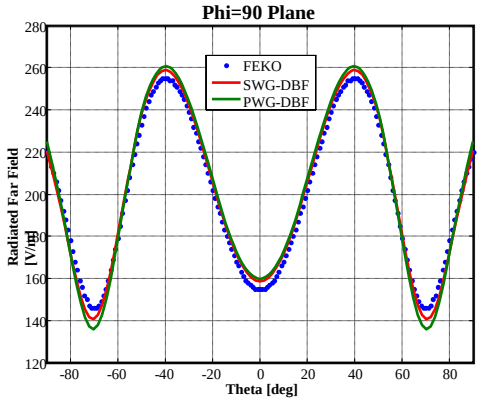

(b)

Fig. 11. Square plate, $L = 0.9\lambda$; far field comparison on (a) E-plane and (b) H-plane.

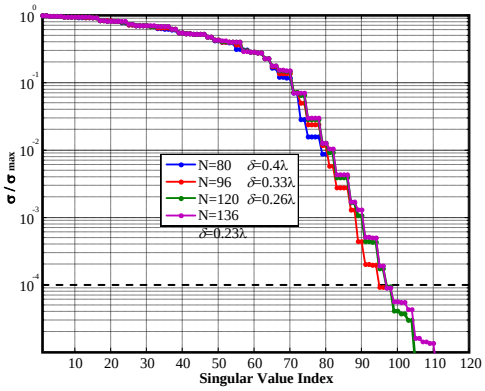

(a)

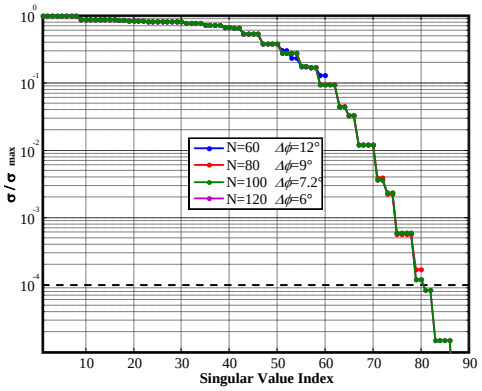

(b)

Fig. 12. SV stabilized sequences for a flat squared metallic plat with side length 4λ (a) Spherical-wave generation (final step $\delta = 0.26\lambda$) (b) Plane-wave generation (final step $\Delta\phi = 7.2°$).

VII. CONCLUDING REMARKS

We have presented a method to reduce the computational cost of the MoM analysis of large and complex structures that exhibits a large portion of flat metallic surfaces with edges. While the overall framework is the one presented in [1] the method is based on breaking down the overall structures into smaller parts, called “blocks,” and constructing entire-domain “synthetic” basis functions over these blocks making use of PO functions to span the solution space. The PO functions are generated by two alternative processes, namely, by using edge located spherical wave sources, or near grazing propagating plane waves. The most evident computational gain consists on a reduction of the MoM matrix size, that have a dimension proportional to the perimeter and not to the area of the plate (it is obvious that this property refers to the description of the edge mechanisms only, and leaves out of consideration the generating sources used for describing the external environment).

Comparison of the two different generating processes shows that the spherical wave generation approach is more accurate while the plane wave generation approach exhibits advantages of closed form spectral domain entries, with favourable capability in treating large structures in terms of wavelengths.

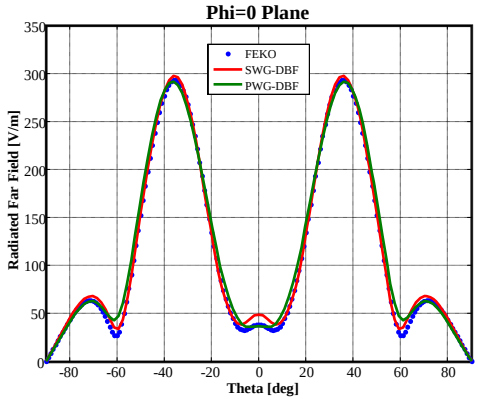

(a)

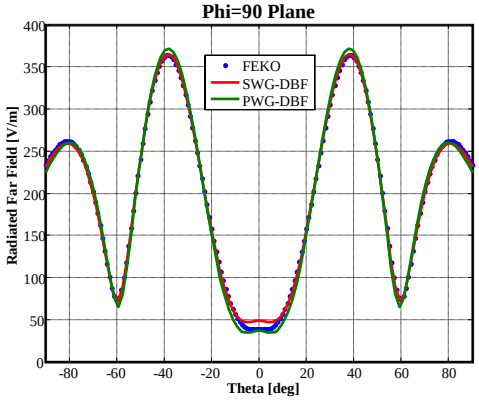

(b)

Fig.13. Square plate, $L = 4\lambda$; far field comparison on E-plane (a) and H-plane (b).

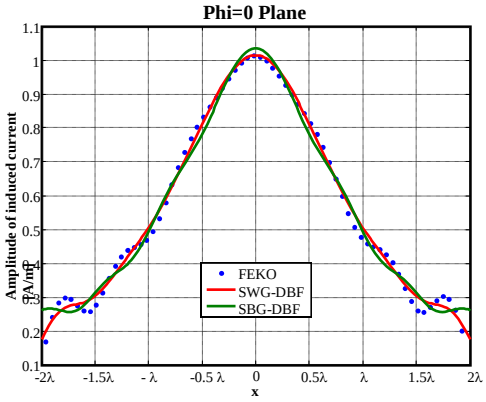

(a)

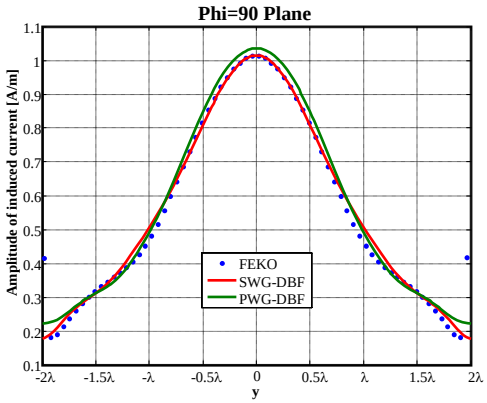

(b)

Fig. 14. Square plate, $L = 4\lambda$; induced currents comparison on E-plane (a) and H-plane cut (b).

REFERENCES

[1] S. Maci, R. Mittra, and G. Vecchi, "A Unified Iteration-Free Approach to Solving Large Antenna and Scattering Problems," *IEEE AP-S Symposium* Washington DC, July 2005, and *IEEE AP-S Symposium* Albuquerque, July 2006.

[2] P. Pirinoli, L. Matekovits, G. Vecchi, F. Vapiana, and M. Orefice, "Synthetic functions: multiscale MoM analysis of arrays," *Proc. of the 2003 IEEE Antennas Propagation Society Symposium*, vol. 4, pp. 799-802, Columbus, 22-27 June 2003.

[3] V. V. S. Prakash and R. Mittra, "Characteristic basis function method: A new technique for fast solution of integral equations," *Micro. Opt. Tech. Lett.*, pp. 95–100, Jan. 2003.

[4] L. Matekovits, V. A. Laza, and G. Vecchi, "Analysis of Large Complex Structures With the Synthetic-Functions Approach" *IEEE Trans. Antennas Propagat.*, vol. 55, no. 9, pp. 2509-2521, Sep. 2007.

[5] S. Maci, M. Albani, and F. Capolino, "ITD Formulation for the Currents on a Plane Angular Sector," *IEEE Trans. Antennas Propagat.*, vol. 46, no. 9, September. 1998.

[6] P. Y. Ufimtsev, *Fundamentals of the Physical Theory of Diffraction*, IEEE Press, Wiley Inter-science, 2007.

[7] O. M. Bucci and G. Franceschetti, "On the degrees of freedom of the scattered fields," *IEEE Trans. Antennas Propagat.*, vol. 37, no. 7, pp. 918-926, July 1989

[8] G. Tiberi, S. Rosace, A. Monorchio, G. Manara, and R. Mittra, "Electromagnetic scattering from large faceted conducting bodies by using analytically derived characteristic basis functions," *IEEE Antennas Wireless Propagat. Lett.*, vol. 2, pp. 290- 293, 2003.

[9] M. Casaletti "Deterministic and Stochastic Methods for the Electromagnetic Analysis of Complex Structures," Ph.D. Thesis, University of Siena, Department of Information Engineering, 2007.

Massimiliano Casaletti was born in Siena, Italy, in 1975. He received the Laurea degree in Telecommunications engineering and the Ph.D. degree in Information engineering from the University of Siena, Italy, in 2003 and 2007, respectively. From September 2003 to October 2005 he has been with the research center MOTHESIM, Les Plessis Robinson (Paris, FR), under a EU grant RTN-AMPER (RTN: Research Training Network, AMPER: Application of Multiparameter Polarimetry). Since 2006, he has been Research Associate at the University of Siena, Italy. His research interests include electromagnetic band-gap structures, polarimetric radar, rough surfaces and numerical methods for electromagnetic scattering and beam waveguides.

Stefano Maci was born in Rome in 1961. Since '98 he joined the University of Siena, Italy, where he presently is a Full Professor. His research interests include: theory of Electromagnetism, high-frequency techniques, integral equation methods, large phased array antennas, planar antennas and multilayer structures, reflector antennas and feed horns, metamaterials. He was a co-author of an Incremental Theory of Diffraction for the description of a wide class of electromagnetic scattering phenomena at high frequency, and of a diffraction theory for the high frequency analysis of large truncated periodic structures. On these subjects he was various times recipient of best paper award in international journals and conferences. In 2004 he was founder, and he presently is the coordinator, of the "European school of antennas" (ESoA), a post-graduate school comprising 12 course per year and 150 teachers coming from 20 European research centres. He was the responsible of several projects funded by the European Union (EU), by the European Space Agency (ESA-ESTEC) and by various European industries; he was work package leader in the Network of Excellence "Antenna Center of Excellence" (FP6, EU). He was associate editor of IEEE Transactions on EMC, and he is associate editor of IEEE Transaction on Antennas and Propagation. He is member of the Technical Advisory Board of the URSI Commission B, member of the Delegate Assembly of the European Association of Antennas and Propagation, member of a NATO panel on metamaterials and MEMS, member of the scientific board of the Italian Society of Electromagnetism (SIEM), and coordinator of the board of the Italian PhD school of Electromagnetism, member of the Board of Director of the European Association of Antennas nd Propagation. He is a Fellow ('04) of IEEE, two times guest editor of special issues of IEEE Transaction on Antennas and Propagation. He is principal author or co-author of about 100 papers published in international journals, 8 book Chapters, and about 300 papers in proceedings of international conferences.

Giuseppe Vecchi received the Laurea and Ph.D. (Dottorato di Ricerca) degrees in electronic engineering from the Politecnico di Torino, Torino, Italy, in 1985 and 1989, respectively, with doctoral research carried out partly at Polytechnic University (Farmingdale, NY). He was a Visiting Scientist with Polytechnic University in 1989-1990. In 1990, he joined the Department of Electronics, Politecnico di Torino, as an Assistant Professor (Ricercatore) where, from 1992 to 2000, he was an Associate Professor and, since 2000, he has been a Professor. He was a Visiting Scientist at the University of Helsinki, Finland, in 1992, and has been an Adjunct Faculty in the Department of Electrical and Computer Engineering, University of Illinois at Chicago, since 1997. His current research activities concern analytical and numerical techniques for analysis, design and diagnostics of antennas and devices, RF plasma heating, electromagnetic compatibility, and imaging.